

# Retinex-MEF: Retinex-based Glare Effects Aware Unsupervised Multi-Exposure Image Fusion

Haowen Bai<sup>1</sup> Jiangshe Zhang<sup>1\*</sup> Zixiang Zhao<sup>2</sup> Lilun Deng<sup>1</sup> Yukun Cui<sup>1</sup> Shuang Xu<sup>3</sup>

<sup>1</sup>Xi'an Jiaotong University <sup>2</sup>ETH Zürich <sup>3</sup>Northwestern Polytechnical University

hwbaii@stu.xjtu.edu.cn

## Abstract

Multi-exposure image fusion consolidates multiple low dynamic range images of the same scene into a singular high dynamic range image. Retinex theory, which separates image illumination from scene reflectance, is naturally adopted to ensure consistent scene representation and effective information fusion across varied exposure levels. However, the conventional pixel-wise multiplication of illumination and reflectance inadequately models the glare effect induced by overexposure. To better adapt this theory for multi-exposure image fusion, we introduce an unsupervised and controllable method termed (**Retinex-MEF**). Specifically, our method decomposes multi-exposure images into separate illumination components and a shared reflectance component, and effectively modeling the glare induced by overexposure. Employing a bidirectional loss constraint to learn the common reflectance component, our approach effectively mitigates the glare effect. Furthermore, we establish a controllable exposure fusion criterion, enabling global exposure adjustments while preserving contrast, thus overcoming the constraints of fixed-level fusion. A series of experiments across multiple datasets, including underexposure-overexposure fusion, exposure control fusion, and homogeneous extreme exposure fusion, demonstrate the effective decomposition and flexible fusion capability of our model. The code will be released.

## 1. Introduction

Current photographic equipment often captures a dynamic range far lower than natural scenes, failing to adapt to large-scale illumination variations in the real world. This results in poor visibility and detail loss [12, 21, 41]. Multi-exposure image fusion (MEIF) merges multiple images from the same scene, taken at different exposure levels, to create a single high dynamic range (HDR) image that retains details in both highlights and shadows, enhancing dy-

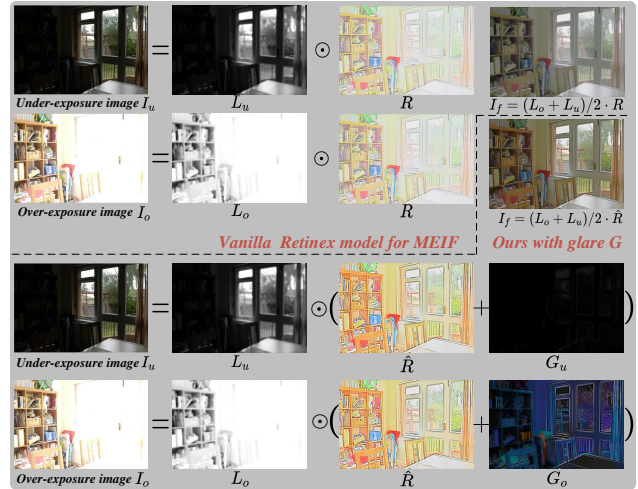


Figure 1. Traditional Retinex-based techniques for multi-exposure image fusion struggle with overexposed regions, which can adversely affect the learning of the reflectance component  $R$ . Our model circumvents this issue by modeling the glare effects  $G$ , effectively restoring the shared reflectance component  $\hat{R}$  and achieving satisfying results.

dynamic range and color accuracy [2, 9, 17, 19, 22, 23, 31, 33, 36, 39, 40, 45]. This technique excels under extreme lighting conditions or when the illumination changes rapidly, offering greater flexibility in capturing scenes [4, 35, 48]. Emerging deep learning-based MEIF techniques, although promising, face limitations as supervised methods depend on ground truths that are artificially selected or synthesized, restricting their effectiveness in accurately capturing scene details and adjusting to natural exposure variations [11, 20, 26, 27, 49, 50, 55]. Unsupervised methods, using feature-level or pixel-level constraints, still suffer from image degradation due to extreme exposures, failing to fully preserve scene information. Overcoming the reliance on ground truth and accurately recovering scene information under extreme exposures remains a significant challenge in MEIF.

Considering that multi-exposure image sequences capture the same scene at different exposure levels, we uti-

\*Corresponding authors.

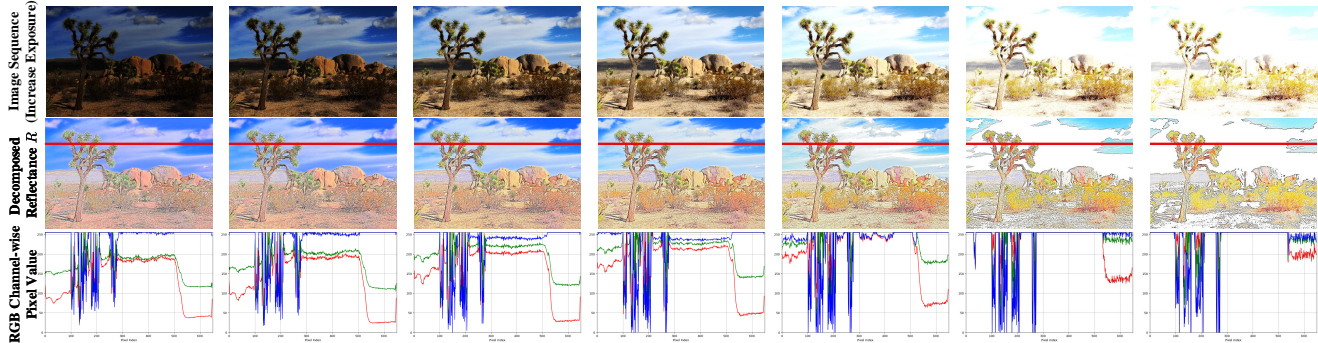


Figure 2. The demonstration of glare effects, as exposure gradually increases, the extraction of the reflectance component in overexposed areas tends toward the maximum value. This results in a coloration that is almost pure white, which subsequently affects the accurate estimation of the scene’s true reflectance component.

lize Retinex theory, which simulates the human visual system’s processing mechanisms to enhance color and brightness. This theory is extensively applied in applications such as low-light enhancement, dynamic range extension, and more [28, 34, 44, 47]. Retinex theory states that an observed image  $I$  is the element-wise product of the illumination component  $L$  and the scene reflectance  $R$ , *i.e.*,  $I = L \cdot R$  [7, 18, 21]. Here,  $L$  represents the scene’s lighting conditions, influenced by the exposure level of a single capture, while  $R$  represents the physical properties of the scene, which remain consistent under different lighting conditions. Within the Retinex framework, multi-exposure image sequences share a common reflectance component that captures the physical properties of the scene, while the primary distinction among the images is their varying exposure levels. Retinex theory effectively decouples exposure conditions from scene information, eliminating the need for manually designed features and allowing scene details to be revealed without relying on ground truth. Moreover, by isolating the illumination component, the fusion process becomes more flexible and targeted, enabling the generation of images that are not confined to any specific exposure level. Thus, this paper addresses the unsupervised MEIF problem using Retinex imaging theory, processing  $L$  and  $R$  separately for more accurate and flexible fusion.

Historically, Retinex theory has been predominantly applied to low-light enhancement, where the degradation primarily results from reduced illumination levels. However, in MEIF, excessive exposure can lead to glare effects, which elevate pixel values and distort the extraction of the reflectance component  $R$ , as demonstrated in Fig. 2. This overexposure disrupts the learning of a consistent  $R$ , causing color shifts and loss of detail in Fig. 1. Therefore, in this paper, we also model the glare phenomenon induced by extreme exposure to accommodate the challenges posed by overexposure in MEIF.

This paper introduces an unsupervised multi-exposure image fusion method utilizing Retinex theory, tailored to address the specific challenges of multi-exposure fusion.

Our framework models glare effects from excessive exposure, allowing the extracted reflectance component  $R$  to align with a shared component  $\hat{R}$  instead of converging [8]. To mitigate glare, we employ a bidirectional loss on  $\hat{R}$  to preserve the scene’s colors and details. Furthermore, we implement a parameterized illumination fusion criterion that ensures brightness variation and fidelity, facilitating customized exposure adjustments across the image. The contributions of this paper are summarized as follows:

- 1) We introduce an effective Retinex-based unsupervised fusion method that separates reflectance from varying exposure levels, enabling precise exposure blending and improved detail preservation.
- 2) We propose a fusion strategy using a symmetric and monotonic function to achieve manually controllable exposure adjustments across the image while ensuring contrast is maintained.
- 3) We tackle the glare issue in overexposure scenarios by discarding traditional pixel-level constraints and applying bidirectional constraints to better model and restore reflectance without glare effects.
- 4) Our algorithm shows excellent fusion performance on public multi-exposure fusion datasets, with exposure control experiments demonstrating its controllability.

## 2. Related Work

### 2.1. Deep learning-based MEIF

In recent years, deep learning-based multi-exposure methods can be categorized into branches of discriminative models [13], generative models [42, 50], and unified fusion models [1, 60]. Discriminative models typically rely on Convolutional Neural Networks (CNNs) [16] or transformers to predict decision maps [13, 32, 32] or directly reconstruct fused images. Supervised learning methods depend on constraints from GT and prior knowledge for effective reconstruction, while unsupervised methods leverage the similarity constraints between the fused image and source images, such as MEF-SSIM [30], to perform regression [38]

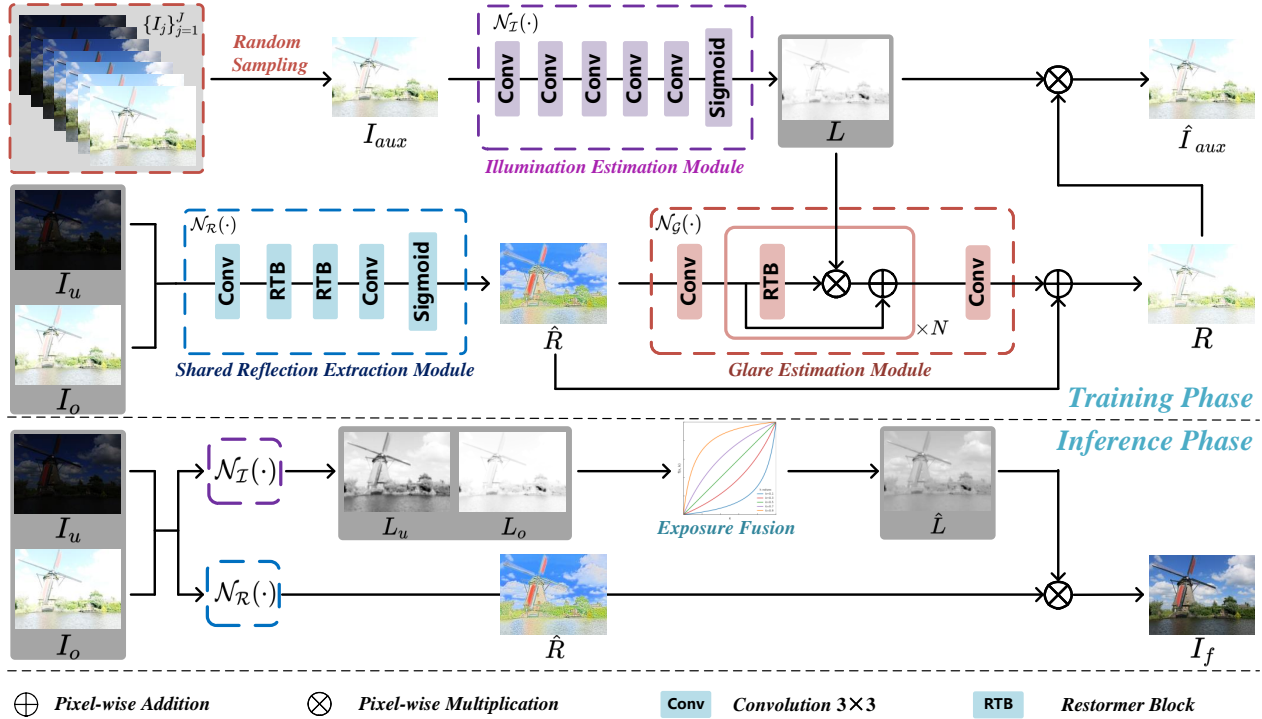


Figure 3. The workflow for the proposed Retinex-MEF method. Our method includes three modules: the Illumination Estimation Module for estimating illumination, the Shared Reflection Extraction Module for extracting the common reflectance component of the scene, and the Glare Estimation Module for glare estimation. An image with a random exposure level from multi-exposure images is sampled in each step, enhancing the ability of each module to estimate different components through Retinex-based decomposition and reconstruction.

and achieve more robust results. Generative models integrate multi-source images at the distribution level, enforcing consistency between the fused image and source images in terms of distribution. These models are often based on Generative Adversarial Networks (GANs) [50] or diffusion denoising models [42]. Unified fusion models [5, 49, 61] also provide insights for multi-exposure image fusion. For instance, they may use the reconstruction of source images from the fused image to aid fusion [1, 54], employ self-supervised methods using masked images to recover the original image, thereby eliminating the need for GT [25], or embed text features from large language models [60] and adaptively learn fusion losses based on the fusion task [1].

## 2.2. Retinex theory

Retinex theory is frequently utilized to enhance low-light conditions. Single-Scale Retinex [15] employs a fixed-scale Gaussian filter to mimic human perception of brightness, improving image contrast and brightness, yet often resulting in color distortion. Multi-Scale Retinex [37] combines filters at multiple scales to better handle image details and colors. In deep learning frameworks, Retinex theory is commonly used to estimate illumination maps and reflectance [6, 10, 46, 57, 59]. Retinexformer enhances images using a Retinex-based transformer, while EnlightenGAN [14] learns the transformation of images from low to

normal lighting conditions using a Generative Adversarial Network, and Diff-Retinex enhances low-light images with a generative diffusion model. Additionally, URetinex [47] explores the use of a Retinex-based deep unfolding network for single-image low-light enhancement, and CRetinex [51] introduces a new color shift-aware Retinex model that focuses on resolving color shift issues under low-light conditions. The most relevant to this paper is the method of single-image low-light enhancement based on Retinex, trained on paired low-light images to explore the common reflectance in multiple underexposed images and enhance them in an unsupervised manner [8]. In this paper, based on Retinex theory, we decouple and separately process the illumination and reflectance of source image pairs. By extracting the common reflectance  $\hat{R}$  that is unaffected by overexposure and controllably fusing illumination from multiple source images, we effectively improve image quality.

## 2.3. Comparison with Existing Approaches

Compared to existing multi-exposure image fusion methods, our approach does not rely on pixel-level constraints of the source images. Instead, we embrace Retinex theory to adjust exposure levels and restore the scene. By modeling the common reflectance component and the glare phenomenon caused by exposure, we restore the common reflectance component  $\hat{R}$  that is unaffected by exposure lev-

els. The adjustable fusion of illumination with  $\hat{R}$  leads to superior performance in image fusion. Unlike previous Retinex-based methods, we address the glare phenomenon under extreme lighting conditions and effectively model it. Through bidirectional loss constraints, we extract the common reflectance component  $\hat{R}$ , providing a more effective Retinex modeling approach for multi-exposure image fusion.

### 3. Method

Our model is capable of handling multi-level exposure inputs. However, for clarity and comparative experimental purposes, we demonstrate using dual-image fusion as an example. Besides the overexposed and underexposed image pairs  $\{I_u, I_o\}$ , our method incorporates an auxiliary input  $I_{aux}$ , derived from the same sequence  $\{I_j\}_{j=1}^J$  as  $\{I_u, I_o\}$ . The decomposition and reconstruction of varying exposure levels within  $I_{aux}$  enhance our method’s ability to develop a more comprehensive and holistic understanding, thereby ensuring accurate estimation of both exposure and reflectance. However, if the image sequence lacks additional exposure levels,  $I_{aux}$  may be either  $I_u$  or  $I_o$ . During the training process of our framework,  $I_{aux}$  is randomly sampled from the original sequence  $\{I_j\}_{j=1}^J$  and can be the same as either  $I_u$  or  $I_o$ .

#### 3.1. Overview

According to Retinex theory, an image  $I$  can be decomposed into the pixel-wise multiplication of illumination  $L$  and reflectance  $R$ :

$$I = L \cdot R. \quad (1)$$

However, in the multi-exposure image fusion, overexposed regions are prone to glare, resulting in significantly shifted pixel values, as illustrated in Fig. 2. To accurately model this glare effect, we formulate the glare effect aware Retinex decomposition as follows:

$$I = L \cdot (\hat{R} + G). \quad (2)$$

Here,  $\hat{R}$  symbolizes the intrinsic information of the scene that remains constant, while  $G > 0$  represents the glare effect induced by exposure. Incorporating  $G$  leads to an increase in pixel values in overexposed regions.

Our model, depicted in Fig. 3, is composed of three main components, each tasked with modeling different aspects of Eq. (2): the illumination estimation module  $\mathcal{N}_{\mathcal{I}}(\cdot)$ , the shared reflectance extraction module  $\mathcal{N}_{\mathcal{R}}(\cdot)$ , which extracts the shared reflectance  $\hat{R}$  from paired images, and the glare estimation module  $\mathcal{N}_{\mathcal{G}}(\cdot)$ , designed to model the glare effect  $G$ . In addressing the multi-exposure image fusion challenge, guided by Retinex theory, we employ neural networks coupled with a series of constraints to model the illumination  $L$  from images with varying exposures and to

recover the intrinsic scene information  $\hat{R}$  affected by these exposures. Following the fusion and adjustment of exposure, the resulting fused exposure  $\hat{L}$  is obtained, and the corresponding fused image is computed as  $I_f = \hat{L} \cdot \hat{R}$ .

#### 3.2. Retinex-MEF

**Estimation of Illumination.** Beyond the underexposed and overexposed image pairs  $I_u, I_o$ , we have another auxiliary image  $I_{aux} \in \{I_j\}_{j=1}^J$ . The exposure level of this auxiliary image is arbitrary and does not require differentiation from  $\{I_u, I_o\}$ , as its primary function is to facilitate the precise estimation of both illumination and reflectance. The illumination extraction network  $\mathcal{N}_{\mathcal{I}}(\cdot)$  is composed of five convolutional layers and a *Sigmoid*( $\cdot$ ) activation function, designed to estimate the single-channel illumination  $L$  of the auxiliary image  $I_{aux}$ :

$$L = \mathcal{N}_{\mathcal{I}}(I_{aux}). \quad (3)$$

**Extraction of Shared Reflectance.** The reflectance extraction module is designed to extract the shared reflectance component  $\hat{R}$  from a pair of images, producing an RGB three-channel output. This component encapsulates the intrinsic physical properties of the scene and effectively filters out glare effects. To accomplish this, the module utilizes a two-layer Restormer block (RTB) [53] for robust feature extraction and precise scene information refinement. The extraction of the shared reflectance component is formulated as follows:

$$\hat{R} = \mathcal{N}_{\mathcal{R}}(I_u, I_o). \quad (4)$$

**Estimation of Glare Component.** The glare estimation module concurrently processes the intrinsically shared reflectance  $\hat{R}$  of the scene and the arbitrary illumination  $L$  as inputs, calculating the glare effect under the current exposure level. In this module, the illumination is directly multiplied with the intermediate features in the  $N$  submodules to embed the illumination information. This is specifically represented as:

$$\Phi_{k+1} = \Phi_k + \text{RTB}(\Phi_k) \cdot L, \quad (5)$$

where  $\Phi_k$  represents the feature of the  $k$ -th submodule. The glare effect modifies  $\hat{R}$ , producing a distorted reflectance  $R$ , which is subsequently combined with the illumination  $L$  to recreate the input image  $I_{aux}$ . This transformation is depicted as follows:

$$R = \hat{R} + \mathcal{N}_{\mathcal{G}}(\hat{R}, L), \quad (6)$$

$$\hat{I}_{aux} = L \cdot R. \quad (7)$$

#### 3.3. Training

Throughout the training phase, the auxiliary image  $I_{aux}$  is randomly selected from the same sequence as the un-

derexposed and overexposed images, and it is concurrently fed into the network together with the underexposed-overexposed image pairs. Our model advances its proficiency by systematically decomposing and reconstructing the auxiliary image  $I_{aux}$ , thereby significantly improving its capabilities in estimating exposure, extracting scene reflectance, and assessing glare effects. To ensure precise decomposition and reconstruction, we implement a series of constraints derived from the Retinex theory. The foremost constraint involves the accurate reconstruction of the input image, which is expressed as

$$\mathcal{L}_{recon} = \|L \cdot R - I_{aux}\|_1. \quad (8)$$

For the illumination component  $L$ , constraints are imposed from two perspectives. Initially, since illumination changes in natural scenes tend to be gradual, applying smoothness constraints to  $L$  is physically justified and facilitates the extraction of high-frequency components from  $R$  [47, 51, 52]. Following the approach in [58], we define the illumination smoothness loss as:

$$\mathcal{L}_{smooth} = \left\| \frac{\nabla_x L}{\max(|\nabla_x I_{aux}|, \xi)} \right\|_1 + \left\| \frac{\nabla_y L}{\max(|\nabla_y I_{aux}|, \xi)} \right\|_1, \quad (9)$$

where  $\nabla_x$  and  $\nabla_y$  denote the gradients in the horizontal and vertical directions, respectively, and  $\xi = 0.01$  to ensure computational stability. Additionally, we constrain illumination  $L$  to approximate the maximum values across the RGB channels, thereby preserving the color information of the scene more effectively. This constraint aims to ensure that the maximum value of the reflectance component remains close to 1, thus preventing distortions from overly high values caused by underestimated illumination and mitigating detail loss in the reflectance component, which can occur when illumination is overestimated [8, 47]. Consequently, we establish a constraint on the initial value  $L_0 = \max_{c \in \{R, G, B\}} I^c(x)$ , as follows:

$$\mathcal{L}_{initialize} = \|L - L_0\|_1. \quad (10)$$

According to Eq. (2), the ground truth for  $\hat{R}$  is designated as  $\hat{R}_{gt}$ , leading to  $I = L \cdot (\hat{R}_{gt} + G)$ . To align  $\hat{R}$  closely with  $\hat{R}_{gt}$ , it is necessary to implement a constraint. Glare effect  $G$  is not consistent across all exposure levels but is predominant in overexposed images. Thus, at lower exposure levels,  $G$  tends towards zero. Consequently, for most instances,  $L \cdot \hat{R}_{gt} \leq L \cdot (\hat{R}_{gt} + G) = I$ , though occasionally,  $L \cdot \hat{R}_{gt} = I$ . By applying the constraint  $L \cdot \hat{R} \leq I$  universally, we ensure that  $\hat{R} \leq \hat{R}_{gt}$ . To enforce this, we introduce a suppression loss that caps the upper limit of  $\hat{R}$ , defined as:

$$\mathcal{L}_{suppress} = \max(0, L \cdot \hat{R} - I). \quad (11)$$

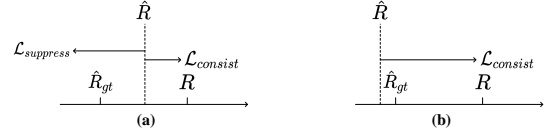


Figure 4. A schematic illustration of the synergistic effect between suppression loss  $\mathcal{L}_{suppress}$  and consistency loss  $\mathcal{L}_{consist}$ . When  $\hat{R}$  exceeds  $\hat{R}_{gt}$ , the two losses conflict, but  $\mathcal{L}_{suppress}$  plays a dominant role. Conversely, when  $\hat{R}$  is less than  $\hat{R}_{gt}$ ,  $\mathcal{L}_{consist}$  ensures that  $\hat{R}$  increases.

The constraint delineated in Eq. (11), which is relevant across all exposure levels, mandates that  $\hat{R} \leq \hat{R}_{gt}$ . Furthermore, in line with the principles of Retinex decomposition, the estimated value of  $R$  should be consistent with  $\hat{R}$  [8, 47, 52]. Thus, we introduce a consistency loss, assigned a lower weight than  $\mathcal{L}_{suppress}$ , to ensure adherence to inherent scene consistency mandated by Retinex theory:

$$\mathcal{L}_{consist} = \|\hat{R} - R\|_1. \quad (12)$$

This loss ensures that the perturbed reflectance  $R$ , extracted at varying exposure levels, remains consistent with the shared reflectance  $\hat{R}$ . Given that  $\hat{R}_{gt} < R$ , the objective of this loss is to maximize  $\hat{R}$  within the bounds set by  $\hat{R}_{gt}$ . The constraints  $\mathcal{L}_{suppress}$  and  $\mathcal{L}_{consist}$  synergistically regulate  $\hat{R}$ , ensuring it closely approximates  $\hat{R}_{gt}$ . On one hand, with both constraints using the  $\ell_1$ -norm but  $\mathcal{L}_{consist}$  assigned a smaller weight than  $\mathcal{L}_{suppress}$ ,  $\mathcal{L}_{suppress}$  predominates in conflicts, maintaining  $\hat{R} \leq \hat{R}_{gt}$ . Conversely, when  $\hat{R} \leq \hat{R}_{gt}$  has been achieved and considering  $\hat{R} \leq R$ ,  $\mathcal{L}_{consist}$  acts to elevate  $\hat{R}$ , guiding it towards convergence with  $\hat{R}_{gt}$ . This synergistic effect is illustrated in Fig. 4.

The total loss for our model is a composite of several distinct loss components, formulated as follows:

$$\mathcal{L}_{total} = \mathcal{L}_{recon} + \alpha_1 \mathcal{L}_{smooth} + \alpha_2 \mathcal{L}_{initialize} + \alpha_3 \mathcal{L}_{suppress} + \alpha_4 \mathcal{L}_{consist}, \quad (13)$$

where  $\alpha_1, \alpha_2, \alpha_3, \alpha_4$  are the weighting coefficients, with  $\alpha_3 > \alpha_4$ .

### 3.4. Inference

During the inference phase, both underexposed and overexposed images  $\{I_u, I_o\}$  are input directly into the  $\mathcal{N}_{\mathcal{R}}(\cdot)$  module to derive the common scene reflectance, represented as  $\hat{R} = \mathcal{N}_{\mathcal{R}}(I_u, I_o)$ . The primary goal of inference is to effectively fuse and adjust the exposure levels. A straightforward method involves averaging the illumination values of the two images to facilitate this fusion:

$$\hat{L} = \frac{L_u + L_o}{2}. \quad (14)$$

Benefiting from the separation of exposure and reflectance components, our objective is to ensure that our fusion

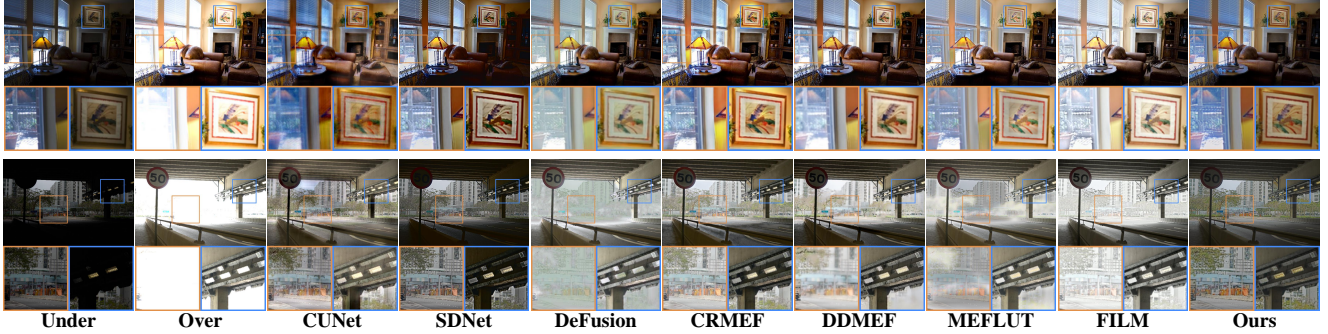


Figure 5. Visual comparison of fused images across different methods. The cases are “Room” in MEFB dataset and “225” in SICE dataset.

Table 1. Quantitative results for two datasets. The red and blue markers represent the best and second-best values, respectively.

	MEFB [56] Multi-Exposure Image Fusion Dataset						SICE [3] Multi-Exposure Image Fusion Dataset					
	$Q_{cb}\uparrow$	NMI $\uparrow$	$Q_{ncie}\uparrow$	SSIM $\uparrow$	PSNR $\uparrow$	CC $\uparrow$	$Q_{cb}\uparrow$	NMI $\uparrow$	$Q_{ncie}\uparrow$	SSIM $\uparrow$	PSNR $\uparrow$	CC $\uparrow$
CUNet [5]	0.444	0.467	0.813	0.897	11.367	0.856	0.435	0.402	0.809	0.872	9.239	0.788
SDNet [54]	0.454	0.734	0.819	0.877	11.225	0.901	0.432	0.625	0.813	0.888	8.720	0.816
DeFusion [24]	0.392	0.777	0.821	0.899	11.621	0.862	0.345	0.573	0.812	0.871	8.501	0.657
CRMEF [29]	0.459	0.658	0.817	0.921	11.785	0.907	0.434	0.526	0.811	0.890	9.488	0.839
DDMEF [43]	0.424	0.621	0.816	0.902	11.843	0.895	0.401	0.528	0.811	0.884	9.347	0.830
MEFLUT [13]	0.460	0.806	0.823	0.884	10.995	0.743	0.394	0.668	0.815	0.885	8.561	0.646
FILM [60]	0.432	0.835	0.822	0.915	10.565	0.896	0.363	0.664	0.813	0.889	7.999	0.838
Ours	0.465	0.855	0.823	0.923	11.856	0.910	0.448	0.671	0.814	0.893	9.508	0.841

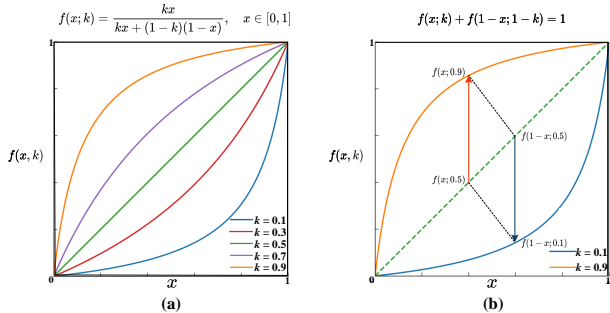


Figure 6. (a) A schematic illustration of the exposure fusion function  $f(x; k)$  at different values of  $k$ . (b) The symmetry of the function  $f(x; k)$  ensures the symmetry of exposure control.

results remain independent of specific exposure levels, thereby allowing for flexible adjustments to global illumination. To achieve this goal, we have developed a controllable exposure fusion function, which is described as follows:

$$f(x; k) = \frac{kx}{kx + (1-k)(1-x)}. \quad (15)$$

In this function,  $x \in [0, 1]$  denotes the pre-adjustment exposure level, while  $k \in [0, 1]$  indicates the desired increase in exposure, serving as an adjustable parameter. Consequently, a higher  $k$  value leads to a brighter image. Behavior of  $f(x)$  across varying  $k$  values is depicted in Fig. 6 (a).

This function possesses several features conducive to adjusting illumination: 1) It is monotonically increasing with respect to both  $x$  and  $k$ , enabling a range of adjustments for varying  $k$  values and simplifying to the identity map-

ping  $f(x) = x$  when  $k = 0.5$ . Additionally, the function fulfills the condition  $f(x; k) + f(1-x; 1-k) = 1$ , as depicted in Fig. 6 (b). This indicates that when the adjustment parameters are  $k$  and  $1-k$ , respectively, the change in pixel value from  $x$  to  $f(x)$  is directly counterbalanced by the change from  $1-x$  to  $f(1-x)$ , aligning with the symmetrical nature of exposure adjustments. To facilitate more nuanced exposure adjustments, we propose a reformulation of Eq.(14) as follows:

$$\hat{L} = f\left(\frac{L_u + L_o}{2}; k\right). \quad (16)$$

In our fusion experiments and visualizations, we fix  $k$  at 0.5, indicating that the illumination adjustment is governed by Eq.(14). For the exposure adjustment and homogeneous extreme exposure fusion experiments, we strictly follow the fusion criteria outlined in Eq.(16). During these adjustments, we define the exposure level  $E$  as the average exposure across the entire image, which is calculated as follows:

$$E = \text{mean}(\hat{L}). \quad (17)$$

For the specified exposure level  $E$ , we can inversely calculate  $k$  using Eq. (16), which enables us to determine the fusion exposure  $\hat{L}$ .

## 4. Experiment

### 4.1. Setup

In our experiments, the network is trained for 80 epochs using the Adam optimizer with a batch size of 8. The hy-



Figure 7. Visualization of exposure level adjustment. The cases are “BarHarborSunrise” and “TreyRatcliff” in MEFB dataset.

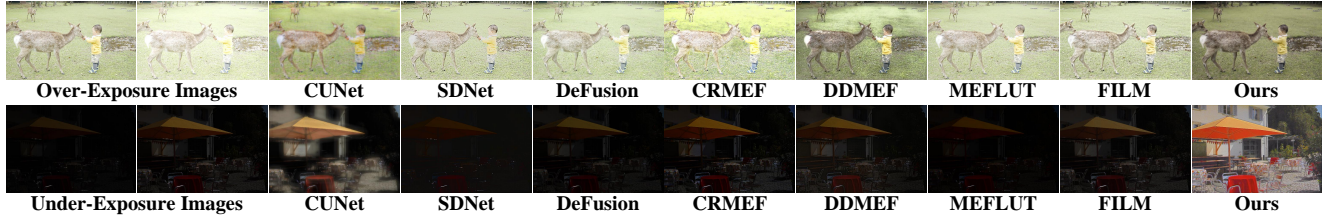


Figure 8. Visual comparison of methods in homogeneous extreme exposure fusion. The top and bottom rows correspond to both overexposure and underexposure inputs, respectively. The cases are “139” and “95” in SICE dataset.

perparameters  $\alpha_1, \alpha_2, \alpha_3, \alpha_4$  are set to 0.5, 0.1, 0.2, 0.1 to ensure the consistency of loss magnitudes and appropriate prioritization. The initial learning rate is established at  $10^{-4}$  and halved every 20 epochs. All experiments are performed on a PC equipped with a single NVIDIA RTX 3090 GPU.

Our method was compared with advanced fusion techniques such as CUNet [5], SDNet [54], DeFusion [24], CRMEF [29], DDMEF [43], MEFLUT [13], and FILM [60]. These fusion techniques were evaluated using metrics such as human visual perception ( $Q_{cb}$ ), normalized mutual information (NMI), nonlinear correlation information entropy ( $Q_{ncie}$ ), the Structural Similarity Index Measure (SSIM) for multi-exposure image fusion, Peak Signal-to-Noise Ratio (PSNR), and the correlation coefficient (CC). The performance was validated using two publicly accessible multi-exposure image fusion datasets SICE [3] and MEFB [56]. A total of 300 image sequences are extracted from the SICE dataset for training and 100 pairs for testing. Furthermore, we incorporated an additional validation set comprising 30 image pairs from the MEFB dataset to further substantiate the model’s performance under varied conditions.

## 4.2. Underexposure-Overexposure Fusion

Tab. 1 showcases a quantitative comparison on two multi-exposure image fusion datasets, where our method outperforms most metrics, excelling in structural preservation and image quality. Results show our approach not only retains key image information effectively but also maintains consistency across various scenarios. Compared to existing methods, ours provides a better balance in structural integrity, information preservation, and contrast enhancement, particularly effective in complex lighting and diverse scenarios, enhancing robustness and adaptability.

Fig. 5 illustrates our method’s visual comparison on two datasets, displaying superior detail preservation in both

overexposed and underexposed areas. In the first indoor scene, details on wall paintings and color layers are richer and clearer than other methods, with a clear outside window scene. In the outdoor scene, textures of roads and buildings are well-preserved. Details like distant trees and railings are notably clearer, with other methods showing blurring. Our glare modeling contributes to a balanced color distribution, preventing over-saturation and color biases, and enhancing visual comfort. More results are displayed in the *supplementary material*.

## 4.3. Exposure Adjustment

Our method excels in controlling exposure, ensuring consistent visual quality across various brightness levels. As shown in Fig. 7, brightness adjusts smoothly through exposure level  $E$ , progressing from 0.1 to 0.9 without abrupt changes or over-enhancement. This allows users to tailor brightness while maintaining the image’s structure and texture. Additionally, our approach ensures color stability and natural appearance across different brightness settings. For instance, as  $E$  changes, the sky retains its natural hue and the colors of the grass and buildings remain vibrant and true, avoiding the color biases typical in HDR methods. More results are displayed in the *supplementary material*.

## 4.4. Homogeneous Extreme Exposure Fusion

Our method dynamically adjusts exposure, unlike traditional methods with fixed targets. By setting  $E = 0.6$ , as demonstrated in Fig. 8, we effectively fuse both underexposed and overexposed image pairs, achieving balanced brightness and natural visuals. Our approach outperforms others in handling extreme exposures: it preserves details in bright areas, such as grass and fur, in overexposed scenes, and enhances dark regions in underexposed scenarios without introducing artifacts or distortions. This flexibility and precision in adjusting to abnormal exposures highlight the

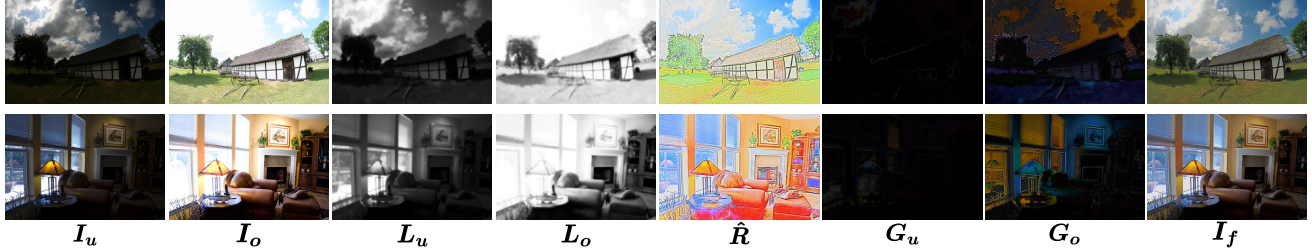


Figure 9. Visualization of the Retinex decomposition results. The cases are “Kluki” and “Room” in MEFB dataset.

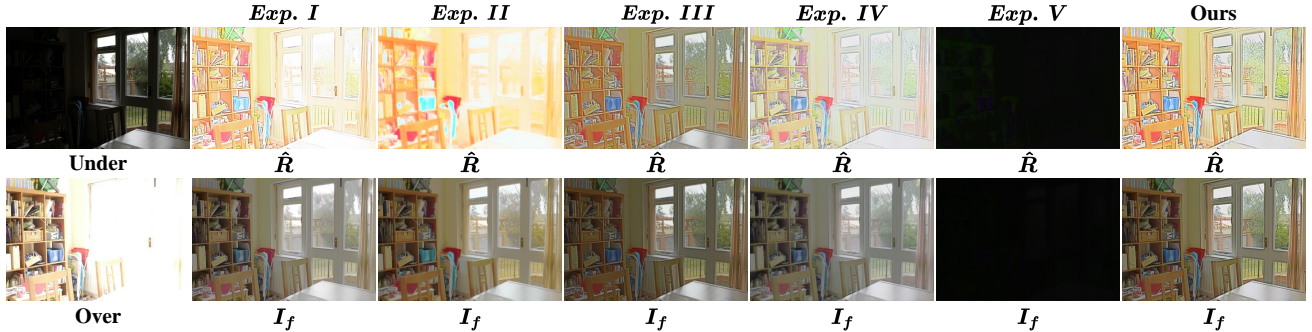


Figure 10. Comparative visualization of different ablation experiments. The case is “House” in MEFB dataset.

robustness and adaptability of our method. More results are displayed in the *supplementary material*.

#### 4.5. Retinex Decomposition

Fig. 9 demonstrates our decomposition approach, successfully separating multiple exposure images into illumination and reflection components. The final fused image  $I_f$  shows an improved balance of brightness and preserved detail. In the reflection component  $\hat{R}$ , our method effectively extracts texture and structural information, eliminates glare effects, and preserves local details like object edges and textures. This modeling of glare effects surpasses direct pixel fusion methods, enhancing the learning of shared reflection components and overall fusion performance. More results are displayed in the *supplementary material*.

#### 4.6. Ablation Study

Our unsupervised method’s performance is significantly influenced by the choice of loss functions, as demonstrated in the ablation studies shown in Fig. 10 and Tab. 2. In Experiment I, applying the reconstruction loss directly to  $\hat{R}$  instead of the glare-affected  $R$  resulted in color degradation. The omission of the smoothness loss in Experiment II led to a reflection component that captured color but lost structural and textural details. Without the initialization loss in Experiment III, the reflection component inadequately preserved colors, darkening the fused image. In Experiment IV, lacking suppression loss caused  $\hat{R}$  to align with the glare-influenced  $R$ , affecting it with overexposure glare. Finally, Experiment V showed that without the consistency loss,  $\hat{R}$  functioned merely as an intermediate feature, failing to produce a fused image. The declines in performance with each

modification, as quantitative results affirm the effectiveness of our method’s loss functions. More visualization results are displayed in the *supplementary material*.

Table 2. Ablation experiment of fusion, the **red** denotes the best.

Ablation Studies of Fusion on MEFB Dataset						
Configurations	$Q_{cb}\uparrow$	NMI $\uparrow$	$Q_{ncie}\uparrow$	MEF $\uparrow$	PSNR $\uparrow$	CC $\uparrow$
I $\mathcal{L}_{recon} =  L \cdot \hat{R} - I_{aux} $	0.411	0.823	0.816	0.909	11.229	0.907
II w/o $\mathcal{L}_{smooth}$	0.435	0.816	0.816	0.910	11.036	0.909
III w/o $\mathcal{L}_{initialize}$	0.443	0.824	0.821	0.892	11.081	0.901
IV w/o $\mathcal{L}_{suppress}$	0.395	0.817	0.816	0.909	11.166	0.905
V w/o $\mathcal{L}_{consist}$	0.290	0.550	0.811	0.511	5.602	0.687
Ours	<b>0.465</b>	<b>0.855</b>	<b>0.823</b>	<b>0.923</b>	<b>11.856</b>	<b>0.910</b>

### 5. Conclusion

To counteract the effects of extreme exposure in source images on multi-exposure image fusion performance, we introduce an unsupervised framework based on Retinex theory. This framework effectively separates and independently refines the common scene reflectance components from the unique exposure levels of each image. By simulating the glare effects in overexposed regions, we safeguard against degradation in these areas, thereby preserving the integrity of common reflectance component extraction through the use of bidirectional constraints. Furthermore, we have developed a controllable exposure fusion function that adapts to various image exposure levels, enabling our model to skillfully blend and adjust exposure level, with flexibility extending beyond producing a single fused image. Experiments on various datasets, including exposure adjustment and fusion of images with abnormal exposures, demonstrate both the effectiveness and flexibility of our model.



## References

- [1] Haowen Bai, Zixiang Zhao, Jianshe Zhang, Yichen Wu, Lilun Deng, Yukun Cui, Baisong Jiang, and Shuang Xu. Refusion: Learning image fusion from reconstruction with learnable loss via meta-learning. *International Journal of Computer Vision*, pages 1–21, 2024. 2, 3
- [2] Neil DB Bruce. Expoblend: Information preserving exposure blending based on normalized log-domain entropy. *Computers & Graphics*, 39:12–23, 2014. 1
- [3] Jianrui Cai, Shuhang Gu, and Lei Zhang. Learning a deep single image contrast enhancer from multi-exposure images. *IEEE Transactions on Image Processing*, 27(4):2049–2062, 2018. 6, 7
- [4] Paul Debevec, Erik Reinhard, Greg Ward, and Sumanta Patanaik. High dynamic range imaging. In *ACM SIGGRAPH 2004 Course Notes*, pages 14–es. 2004. 1
- [5] Xin Deng and Pier Luigi Dragotti. Deep convolutional neural network for multi-modal image restoration and fusion. *IEEE transactions on pattern analysis and machine intelligence*, 43(10):3333–3348, 2020. 3, 6, 7
- [6] Huiyuan Fu, Wenkai Zheng, Xiangyu Meng, Xin Wang, Chuanming Wang, and Huadong Ma. You do not need additional priors or regularizers in retinex-based low-light image enhancement. In *Proceedings of the IEEE/CVF Conference on Computer Vision and Pattern Recognition*, pages 18125–18134, 2023. 3
- [7] Xueyang Fu, Delu Zeng, Yue Huang, Xiao-Ping Zhang, and Xinghao Ding. A weighted variational model for simultaneous reflectance and illumination estimation. In *Proceedings of the IEEE conference on computer vision and pattern recognition*, pages 2782–2790, 2016. 2
- [8] Zhenqi Fu, Yan Yang, Xiaotong Tu, Yue Huang, Xinghao Ding, and Kai-Kuang Ma. Learning a simple low-light image enhancer from paired low-light instances. In *Proceedings of the IEEE/CVF conference on computer vision and pattern recognition*, pages 22252–22261, 2023. 2, 3, 5
- [9] A Ardeshir Goshtasby. Fusion of multi-exposure images. *Image and Vision Computing*, 23(6):611–618, 2005. 1
- [10] Xiaojie Guo, Yu Li, and Haibin Ling. Lime: Low-light image enhancement via illumination map estimation. *IEEE Transactions on image processing*, 26(2):982–993, 2016. 3
- [11] Dong Han, Liang Li, Xiaojie Guo, and Jiayi Ma. Multi-exposure image fusion via deep perceptual enhancement. *Information Fusion*, 79:248–262, 2022. 1
- [12] Li Huang, Zhengping Li, Chao Xu, and Bo Feng. Multi-exposure image fusion based on feature evaluation with adaptive factor. *IET Image Processing*, 15(13):3211–3220, 2021. 1
- [13] Ting Jiang, Chuan Wang, Xinpeng Li, Ru Li, Haoqiang Fan, and Shuaicheng Liu. Meflut: Unsupervised 1d lookup tables for multi-exposure image fusion. In *Proceedings of the IEEE/CVF International Conference on Computer Vision*, pages 10542–10551, 2023. 2, 6, 7
- [14] Yifan Jiang, Xinyu Gong, Ding Liu, Yu Cheng, Chen Fang, Xiaohui Shen, Jianchao Yang, Pan Zhou, and Zhangyang Wang. Enlightengan: Deep light enhancement without paired supervision. *IEEE transactions on image processing*, 30:2340–2349, 2021. 3
- [15] Daniel J Jobson, Zia-ur Rahman, and Glenn A Woodell. Properties and performance of a center/surround retinex. *IEEE transactions on image processing*, 6(3):451–462, 1997. 3
- [16] Nima Khademi Kalantari, Ravi Ramamoorthi, et al. Deep high dynamic range imaging of dynamic scenes. *ACM Trans. Graph.*, 36(4):144–1, 2017. 2
- [17] Fei Kou, Zhengguo Li, Changyun Wen, and Weihai Chen. Multi-scale exposure fusion via gradient domain guided image filtering. In *2017 IEEE international conference on multimedia and expo (ICME)*, pages 1105–1110. IEEE, 2017. 1
- [18] Edwin H Land. The retinex theory of color vision. *Scientific american*, 237(6):108–129, 1977. 2
- [19] Sang-hoon Lee, Jae Sung Park, and Nam Ik Cho. A multi-exposure image fusion based on the adaptive weights reflecting the relative pixel intensity and global gradient. In *2018 25th IEEE international conference on image processing (ICIP)*, pages 1737–1741. IEEE, 2018. 1
- [20] Jiawei Li, Jinyuan Liu, Shihua Zhou, Qiang Zhang, and Nikola K Kasabov. Learning a coordinated network for detail-refinement multiexposure image fusion. *IEEE Transactions on Circuits and Systems for Video Technology*, 33(2):713–727, 2022. 1
- [21] Mading Li, Jiaying Liu, Wenhan Yang, Xiaoyan Sun, and Zongming Guo. Structure-revealing low-light image enhancement via robust retinex model. *IEEE transactions on image processing*, 27(6):2828–2841, 2018. 1, 2
- [22] Shutao Li, Xudong Kang, and Jianwen Hu. Image fusion with guided filtering. *IEEE Transactions on Image processing*, 22(7):2864–2875, 2013. 1
- [23] Zheng Guo Li, Jing Hong Zheng, and Susanto Rahardja. Detail-enhanced exposure fusion. *IEEE Transactions on Image Processing*, 21(11):4672–4676, 2012. 1
- [24] Pengwei Liang, Junjun Jiang, Xianming Liu, and Jiayi Ma. Fusion from decomposition: A self-supervised decomposition approach for image fusion. In *Proceedings of the European Conference on Computer Vision (ECCV)*, pages 719–735, 2022. 6, 7
- [25] Pengwei Liang, Junjun Jiang, Xianming Liu, and Jiayi Ma. Fusion from decomposition: A self-supervised decomposition approach for image fusion. In *European Conference on Computer Vision*, pages 719–735. Springer, 2022. 3
- [26] Jinyuan Liu, Jingjie Shang, Risheng Liu, and Xin Fan. Attention-guided global-local adversarial learning for detail-preserving multi-exposure image fusion. *IEEE Transactions on Circuits and Systems for Video Technology*, 32(8):5026–5040, 2022. 1
- [27] Jinyuan Liu, Guanyao Wu, Junsheng Luan, Zhiying Jiang, Risheng Liu, and Xin Fan. Holoco: Holistic and local contrastive learning network for multi-exposure image fusion. *Information Fusion*, 95:237–249, 2023. 1
- [28] Risheng Liu, Long Ma, Jiaao Zhang, Xin Fan, and Zhongxuan Luo. Retinex-inspired unrolling with cooperative prior architecture search for low-light image enhancement. In *Proceedings of the IEEE/CVF conference on computer vision and pattern recognition*, pages 10561–10570, 2021. 2

- [29] Zhu Liu, Jinyuan Liu, Guanyao Wu, Zihang Chen, Xin Fan, and Risheng Liu. Searching a compact architecture for robust multi-exposure image fusion. *IEEE Transactions on Circuits and Systems for Video Technology*, 34(7):6224–6237, 2024. 6, 7
- [30] Kede Ma, Kai Zeng, and Zhou Wang. Perceptual quality assessment for multi-exposure image fusion. *IEEE Transactions on Image Processing*, 24(11):3345–3356, 2015. 2
- [31] Kede Ma, Hui Li, Hongwei Yong, Zhou Wang, Deyu Meng, and Lei Zhang. Robust multi-exposure image fusion: a structural patch decomposition approach. *IEEE Transactions on Image Processing*, 26(5):2519–2532, 2017. 1
- [32] Kede Ma, Zhengfang Duanmu, Hanwei Zhu, Yuming Fang, and Zhou Wang. Deep guided learning for fast multi-exposure image fusion. *IEEE Transactions on Image Processing*, 29:2808–2819, 2019. 2
- [33] Tom Mertens, Jan Kautz, and Frank Van Reeth. Exposure fusion. In *15th Pacific Conference on Computer Graphics and Applications (PG'07)*, pages 382–390. IEEE, 2007. 1
- [34] L. Meylan and S. Susstrunk. High dynamic range image rendering with a retinex-based adaptive filter. *IEEE Transactions on Image Processing*, 15(9):2820–2830, 2006. 2
- [35] Frosti Palsson, Johannes R Sveinsson, and Magnus O Ulfarsson. Multispectral and hyperspectral image fusion using a 3-d-convolutional neural network. *IEEE Geoscience and Remote Sensing Letters*, 14(5):639–643, 2017. 1
- [36] Sujoy Paul, Ioana S Sevcenco, and Panajotis Agathoklis. Multi-exposure and multi-focus image fusion in gradient domain. *Journal of Circuits, Systems and Computers*, 25(10):1650123, 2016. 1
- [37] Zia-ur Rahman, Daniel J Jobson, and Glenn A Woodell. Multi-scale retinex for color image enhancement. In *Proceedings of 3rd IEEE international conference on image processing*, pages 1003–1006. IEEE, 1996. 3
- [38] K Ram Prabhakar, V Sai Srikar, and R Venkatesh Babu. Deepfuse: A deep unsupervised approach for exposure fusion with extreme exposure image pairs. In *Proceedings of the IEEE international conference on computer vision*, pages 4714–4722, 2017. 2
- [39] Hua Shao, Gangyi Jiang, Mei Yu, Yang Song, Hao Jiang, Zongju Peng, and Feng Chen. Halo-free multi-exposure image fusion based on sparse representation of gradient features. *Applied Sciences*, 8(9):1543, 2018. 1
- [40] Rui Shen, Irene Cheng, Jianbo Shi, and Anup Basu. Generalized random walks for fusion of multi-exposure images. *IEEE Transactions on Image Processing*, 20(12):3634–3646, 2011. 1
- [41] Rui Shen, Irene Cheng, and Anup Basu. Qoe-based multi-exposure fusion in hierarchical multivariate gaussian crf. *IEEE Transactions on Image Processing*, 22(6):2469–2478, 2012. 1
- [42] Yu Shi, Yu Liu, Juan Cheng, Z Jane Wang, and Xun Chen. Vdmufusion: A versatile diffusion model-based unsupervised framework for image fusion. *IEEE Transactions on Image Processing*, 2024. 2, 3
- [43] Xiao Tan, Huaian Chen, Rui Zhang, Qihan Wang, Yan Kan, Jinjin Zheng, Yi Jin, and Enhong Chen. Deep multi-exposure image fusion for dynamic scenes. *IEEE Transactions on Image Processing*, 32:5310–5325, 2023. 6, 7
- [44] Ping Wang, Zhiwen Wang, Dong Lv, Chanlong Zhang, and Yuhang Wang. Low illumination color image enhancement based on gabor filtering and retinex theory. *Multimedia Tools and Applications*, 80:17705–17719, 2021. 2
- [45] Xin Wang, Siqiu Shen, Chen Ning, Fengchen Huang, and Hongmin Gao. Multi-class remote sensing object recognition based on discriminative sparse representation. *Applied optics*, 55(6):1381–1394, 2016. 1
- [46] Chen Wei, Wenjing Wang, Wenhan Yang, and Jiaying Liu. Deep retinex decomposition for low-light enhancement. *arXiv preprint arXiv:1808.04560*, 2018. 3
- [47] Wenhui Wu, Jian Weng, Pingping Zhang, Xu Wang, Wenhan Yang, and Jianmin Jiang. Uretinex-net: Retinex-based deep unfolding network for low-light image enhancement. In *Proceedings of the IEEE/CVF conference on computer vision and pattern recognition*, pages 5901–5910, 2022. 2, 3, 5
- [48] Lu Xing, Lei Cai, Huanqiang Zeng, Jing Chen, Jianqing Zhu, and Junhui Hou. A multi-scale contrast-based image quality assessment model for multi-exposure image fusion. *Signal Processing*, 145:233–240, 2018. 1
- [49] Han Xu, Jiayi Ma, Junjun Jiang, Xiaojie Guo, and Haibin Ling. U2fusion: A unified unsupervised image fusion network. *IEEE transactions on pattern analysis and machine intelligence*, 44(1):502–518, 2020. 1, 3
- [50] Han Xu, Jiayi Ma, and Xiao-Ping Zhang. Mef-gan: Multi-exposure image fusion via generative adversarial networks. *IEEE Transactions on Image Processing*, 29:7203–7216, 2020. 1, 2, 3
- [51] Han Xu, Hao Zhang, Xunpeng Yi, and Jiayi Ma. Cretinex: A progressive color-shift aware retinex model for low-light image enhancement. *International Journal of Computer Vision*, 132(9):3610–3632, 2024. 3, 5
- [52] Xunpeng Yi, Han Xu, Hao Zhang, Linfeng Tang, and Jiayi Ma. Diff-retinex: Rethinking low-light image enhancement with a generative diffusion model. In *Proceedings of the IEEE/CVF International Conference on Computer Vision*, pages 12302–12311, 2023. 5
- [53] Syed Waqas Zamir, Aditya Arora, Salman Khan, Munawar Hayat, Fahad Shahbaz Khan, and Ming-Hsuan Yang. Restormer: Efficient transformer for high-resolution image restoration. In *Proceedings of the IEEE/CVF conference on computer vision and pattern recognition*, pages 5728–5739, 2022. 4
- [54] Hao Zhang and Jiayi Ma. Sdnet: A versatile squeeze-and-decomposition network for real-time image fusion. *International Journal of Computer Vision*, 129(10):2761–2785, 2021. 3, 6, 7
- [55] Hao Zhang, Han Xu, Yang Xiao, Xiaojie Guo, and Jiayi Ma. Rethinking the image fusion: A fast unified image fusion network based on proportional maintenance of gradient and intensity. In *Proceedings of the AAAI conference on artificial intelligence*, pages 12797–12804, 2020. 1
- [56] Xingchen Zhang. Benchmarking and comparing multi-exposure image fusion algorithms. *Information Fusion*, 74:111–131, 2021. 6, 7

- [57] Yonghua Zhang, Jiawan Zhang, and Xiaojie Guo. Kindling the darkness: A practical low-light image enhancer. In *Proceedings of the 27th ACM international conference on multimedia*, pages 1632–1640, 2019. [3](#)
- [58] Yonghua Zhang, Xiaojie Guo, Jiayi Ma, Wei Liu, and Jiawan Zhang. Beyond brightening low-light images. *International Journal of Computer Vision*, 129:1013–1037, 2021. [5](#)
- [59] Zunjin Zhao, Bangshu Xiong, Lei Wang, Qiaofeng Ou, Lei Yu, and Fa Kuang. Retinexdip: A unified deep framework for low-light image enhancement. *IEEE Transactions on Circuits and Systems for Video Technology*, 32(3):1076–1088, 2021. [3](#)
- [60] Zixiang Zhao, Lilun Deng, Haowen Bai, Yukun Cui, Zhipeng Zhang, Yulun Zhang, Haotong Qin, Dongdong Chen, Jianshe Zhang, Peng Wang, et al. Image fusion via vision-language model. *arXiv preprint arXiv:2402.02235*, 2024. [2](#), [3](#), [6](#), [7](#)
- [61] Pengfei Zhu, Yang Sun, Bing Cao, and Qinghua Hu. Task-customized mixture of adapters for general image fusion. In *Proceedings of the IEEE/CVF conference on computer vision and pattern recognition*, pages 7099–7108, 2024. [3](#)